

Contents lists available at ScienceDirect

Journal of Inorganic Biochemistry

journal homepage: www.elsevier.com/locate/jinorgbio





Ruthenium pincer complexes for light activated toxicity: Lipophilic groups enhance toxicity

Yifei Sun^{a,1}, Sanjit Das^{b,1}, Spenser R. Brown^a, Emily R. Blevins^b, Fengrui Qu^a, Nicholas A. Ward^b, Shawn Aiden Gregory^b, Chance M. Boudreaux^b, Yonghyun Kim^{a,*}, Elizabeth T. Papish^{b,*}

ARTICLE INFO

Keywords: Ruthenium Anticancer Light activation Pincer ligands Lipophilic ligands N-heterocyclic carbenes

ABSTRACT

Nine ruthenium CNC pincer complexes (1–9) were tested for anticancer activity in cell culture under both dark and light conditions. These complexes included varied CNC pincer ligands including OH, OMe, or Me substituents on the pyridyl ring and wingtip N-heterocyclic carbene (NHC) groups which varied as methyl (Me), phenyl (Ph), mesityl (Mes), and 2,6-diisopropylphenyl (Dipp). The supporting ligands included acetonitrile, Cl, and 2,2'-bipyridine (bpy) donors. The synthesis of complexes 8 and 9 is described herein and are fully characterized by spectroscopic (1 H NMR, IR, UV–Vis, MS) and analytical techniques. Single crystal X-ray diffraction results are reported herein for 8 and 9. The other complexes (1–7) are reported elsewhere. The four most lipophilic ruthenium complexes (6, 7, 8, and 9) showed the best activity vs. MCF7 cancer cells with complexes 6 and 9 showing cytotoxicity and complex 7 and 8 showing light activated photocytotoxicity. The distribution of these compounds between octanol and water is reported as $\log(D_{0/w})$ values, and increasing $\log(D_{0/w})$ values correlate roughly with improved activity vs. cancer cells. Overall, lipophilic wingtip groups (e.g. Ph, Mes, Dipp) on the NHC ring and a lower cationic charge (1+ vs. 2+) appears to be beneficial for improved anticancer activity.

1. Introduction

Ruthenium-based, light-activated compounds have shown great promise as anticancer agents. We have had a long-standing interest in this area, and we have typically employed tris bidentate imine ligands to form C_2 symmetric complexes. [1–7] These ruthenium complexes [(N, N) $_2$ Ru(n,n'-dhbp)]Cl $_2$ (where N,N = bathophenanthroline or similar ligands, and n,n'-dhbp = 4,4'-dihydroxybipyridine or 6,6'-dihydroxybipyridine) have been chiral, but they were employed for cellular studies as a 50/50 mixture of both enantiomers. [2,3,7] Of course, there

is the possibility that one enantiomer is biologically active, and the other enantiomer is inactive. There is interest in the literature in moving away from chiral scaffolds and instead of using compounds with an internal mirror plane (with C_{2v} or C_s symmetry, for example) such that the compounds are achiral. [8]

In this work, we tested several compounds with approximate C_s symmetry (Fig. 1) in cancer cells in order to elucidate structure-function relationships. Complex 1 has been previously reported [9] and uses a pyridinol derived CNC pincer ligand, to determine if protic pincer ligands show cytotoxicity. Ruthenium complexes 2 and 3 use an

Abbreviations: Å, Angstrom (10^{-10} m); ATR, Attenuated Total Reflectance; A, Absorbance; bpy, 2,2'-bipyridine; CNC, Tridentate pincer ligand with Carbon (C), Nitrogen (N), and Carbon (C) binding sites for the metal center; Dhbp, Dihydroxybipyridine; Dipp, 2,6-diisopropylphenyl; DMSO, Dimethyl sulfoxide; EC_{50} , Half maximal effective concentration; ESI, Electron spray ionization; FTIR, Fourier Transform Infrared spectroscopy; HeLa, A cervical cancer cell line derived from Henrietta Lacks; HRMS, High resolution mass spectrometry; $Log(D_{0/w})$, Distribution coefficient in octanol vs. water; MCF7, A breast cancer cell line (Michigan Cancer Foundation-7); MCF10A, A "normal-like" breast cell line (Michigan Cancer Foundation-10A); MDA-MB-231, A breast cancer cell line (MD Anderson Metastatic Breast cancer-231); Me, Methyl; Mes, Mesityl = 2, 4, 6-trimethylphenyl; NHC, N-heterocyclic carbene; NMR, Nuclear magnetic resonance spectroscopy; Ph, Phenyl; PI, Phototoxicity index = $EC_{50 \text{ dark}}$ / $EC_{50 \text{ light}}$; py, Pyridyl; SC-XRD, Single crystal X-ray diffraction.

E-mail addresses: ykim@eng.ua.edu (Y. Kim), etpapish@ua.edu (E.T. Papish).

^a The University of Alabama, Department of Chemical and Biological Engineering, Tuscaloosa, AL 35487, USA

^b The University of Alabama, Department of Chemistry and Biochemistry, Tuscaloosa, AL 35487, USA

^{*} Corresponding authors.

¹ Equal author contributions.

imidazole derived N-heterocyclic carbene (NHC) ligand and a methoxy group on the pyridine ring. 2,2'-Bipyridine and a monodentate ligand, chloride or acetonitrile, completes the coordination sphere in 2 and 3, respectively. This results in a complex charge of cationic for 2 and dicationic for 3. Similarly, 4 and 5 are analogous to 2 and 3, but 4 and 5 feature a benzimidazole derived NHC ligand in the CNC pincer. The benzimidazole ring should improve lipophilic properties and cellular uptake for these complexes. Inclusion of phenyl (Ph) wingtips on the CNC pincer in 6 and 7 produces even more lipophilic complexes which have been previously reported. [10] Finally, the use of bulky aryl groups was explored in 8 and 9. For reasons of synthetic convenience, complexes 8 and 9 use H or methyl (Me) as the substituent on the pyridine ring in the CNC pincer and feature an imidazole derived NHC ring. Complexes 8 and 9 are cations with Cl and bpy completing the coordination sphere.

Thus, we have studied three known complexes (1, 6, 7) [9,10] and six new complexes (2-5, 8, 9) for their cytotoxicity under both light and dark conditions. Synthetic details and complete characterization data including single crystal X-ray diffraction (SC-XRD) are reported here for complexes 8 and 9, and those of complexes 2-5 are reported separately. [11,12] Screening data under both light and dark conditions indicates that 1-5 are non-toxic or of very low toxicity to the breast cancer cell line MCF7 (Fig. S17). Two complexes (7 and 8) were light activated and showed photocytotoxicity and two complexes were equally cytotoxic under both light and dark conditions (6 and 9). There appears to be a trend of increasing toxicity with more lipophilic organic ligands. Herein, we quantify lipophilic vs. hydrophilic properties by measuring $\log(D_{0/w})$ values at pH 7.4. The distribution coefficient measures the partitioning of a given Ru complex between octanol and water $(D_{0/w})$. Lipophilic

complexes display positive $\log(D_{o/w})$ values that are ideally between 2 and 6 for good cellular uptake and with sufficient water solubility for drug administration. [13–16] Thus, we aim to elucidate promising functional scaffolds for anticancer activity, and we plan to work towards further improvement of the structures and study the mode(s) of action in subsequent studies.

2. Materials and methods

2.1. Materials and instrumentation

1-Octanol (99.99%) was purchased from Acros Organics and used without further purification. Compounds 1–7 were synthesized using published methods without modification or using a procedure that will be submitted for publication. [9–12] Buffer solutions for $\text{Log}(D_{\text{O/w}})$ measurements were prepared fresh at 0.1 M phosphate (pH 7.4). UV–Visible spectra were collected on a Perkin Elmer Lambda 35 spectrometer or a JASCO spectrometer and measured in the range of 200–800 nm.

2.2. Synthesis and characterization

2.2.1. Synthesis of 8

Complex 8 was made in three steps as shown in Scheme 1.

2.2.1.1. Synthesis of 10_{Br} Preligand 10_{Br} was synthesized according to a literature procedure as shown in Scheme 1. [17]

2.2.1.2. Synthesis of 10_{OTf} : 10_{Br} (0.290 g, 0.476 mmol, 1.0 equiv.) was

Fig. 1. Chemical structures of the ruthenium complexes tested for cytotoxicity and photocytotoxicity.

Scheme 1. Synthetic scheme for 8 and 9.

dissolved in a mixture of acetonitrile (20 mL) and ethanol (10 mL) in a round bottomed flask. To this solution was added a solution of CF₃SO₃Ag (0.245 g, 0.952 mmol, 2.0 equiv.) in acetonitrile (10 mL) and the resulting mixture was stirred at room temperature in N₂ environment for 3 h. Then the reaction mixture was filtered through a celite plug, filtrate was evaporated to dryness and the residue was triturated with acetonitrile (1 mL) and diethyl ether (15 mL) to get an off-white solid. The solid was further washed with diethyl ether (15 mL) to obtain the desired product (10_{OTf}) (0.330 g, 0.441 mmol, 93%). *Characterization data for* 10_{OTf}. ¹H NMR (DMSO- d_6 , 360 MHz): δ 10.55 (s, 2H, Im (*pre-carbene H*)); 9.12 (s, 2H, Im); 8.71 (t, 1H, $J_{\rm HH}$ = 7.9 Hz, py); 8.35 (d, 2H, $J_{\rm HH}$ = 7.9 Hz, py); 8.31 (s, 2H, Im); 7.22 (s, 4H, Mes-Ar); 2.36 (s, 6H, Mes-Ar); 2.13 (s, 12H, Mes-Ar). ¹⁹F NMR (DMSO- d_6 , 339 MHz): δ –77.76.

2.2.1.3. Synthesis of **8**. This compound was synthesized starting with Ru(bipy)Cl₄ (0.150 g, 0.376 mmol, 1.0 equiv., prepared by a literature procedure [18]), **10**_{OTf} (0.309 g, 0.413 mmol, 1.1 equiv.), and ethylene glycol (4 mL). The crude material was purified by column (silica gel) chromatography using 0–10% methanol in dichloromethane. It was further purified by recrystallization from vapor diffusion of diethyl ether into acetonitrile solution of the compound to get brown solid as the desired product (**8**) (0.115 g, 0.129 mmol, 34%). Single crystals were grown by vapor diffusion of diethyl ether into acetonitrile solution of the compound. *Characterization data for* **8**: ¹H NMR (DMSO- d_6 , 360 MHz): δ 9.19 (d, 1H, $J_{\rm HH}$ = 6.0 Hz, bpy); 8.69 (d, 2H, $J_{\rm HH}$ = 2.0 Hz, Im); 8.26–8.23 (m, 1H, py); 8.17–8.15 (m, 2H, py); 8.08 (d, 1H, $J_{\rm HH}$ = 8.0 Hz, bpy); 7.71 (t, 1H, $J_{\rm HH}$ = 8.0 Hz, bpy); 7.68 (d, 1H, $J_{\rm HH}$ = 8.0 Hz, bpy);

7.57 (t, 1H, $J_{\rm HH}$ = 8.0 Hz, bpy); 7.45 (d, 1H, $J_{\rm HH}$ = 6.0 Hz, bpy); 7.43 (d, 2H, $J_{\rm HH}$ = 2.0 Hz, Im); 7.05 (t, 1H, $J_{\rm HH}$ = 6.5 Hz, bpy); 6.98 (t, 1H, $J_{\rm HH}$ = 6.5 Hz, bpy); 6.36 (s, 2H, Mes-Ar); 6.29 (s, 2H, Mes-Ar); 2.03 (s, 6H, Mes-Me); 2.00 (s, 6H, Mes-Me); 0.65 (s, 6H, Mes-Me). ¹⁹F NMR (DMSO- d_6 , 339 MHz): δ -77.76. HRMS (ESI, positive) calculated for RuC₃₉H₃₇N₇Cl [M - (CF₃SO₃)]⁺: 740.1842 and found 740.1848. Elemental compositions calculated for RuC₄₀H₃₇N₇O₃F₃ClS (M): C = 54.02%, H = 4.19%, N = 11.02%; found C = 53.95%, H = 4.12%, N = 11.06%. UV-vis: $\lambda_{\rm max}$ = 471 nm, ε = 8300 M⁻¹ cm⁻¹. FTIR (ATR, cm⁻¹): 3121, 3073, 2917, 2859, 1612, 1575, 1548, 1483, 1465, 1446, 1408, 1383, 1308, 1292, 1257, 1237, 1221, 1182, 1160, 1145, 1114, 1098, 1029, 967, 930, 872, 857, 786, 764, 739, 706, 687, 661, 636, 591, 572, 516, 478, 424.

2.2.2. Synthesis of 9

Complex **9** was made in three steps as shown in Scheme **1**.

2.2.2.1. Synthesis of 11_{Cl} . This compound was synthesized following the similar procedure for 10_{Br} (Scheme 1) starting from 1-(2,6-diisopropylphenyl)-1H-imidazol (1.50 g, 6.57 mmol). The crude reaction mixture was purified by column (silica gel) chromatography using 0–30% methanol in dichloromethane to isolate the product (most polar spot on the TLC) as a brownish sticky solid. The solid was triturated with diethyl ether (3 × 5 mL) to get the desired product (11_{Cl}) as an off-white solid (0.326 g, 0.526 mmol, 20%). Characterization data for 11_{Cl} : 1 H NMR (CDCl₃, 360 MHz, ppm): 12.49 (m, 2H, Im (pre-carbene H)); 9.94 (m, 2H, Im); 8.96 (s, 2H, py); 7.51 (t, 2H, J_{HH} = 7.9 Hz, Dipp-Ar); 7.31–7.29 (m, 6H, merged peaks, Dipp-Ar & Im); 2.65 (s, 3H, py-Me); 2.41 (m, 4H, Dipp- $CHMe_2$); 1.27 (d, 12H, J_{HH} = 6.8 Hz, Dipp- $CHMe_2$);

1.15 (d, 12H, $J_{HH} = 6.8$ Hz, Dipp-CHMe₂).

2.2.2.2. Synthesis of 11_{OTf} . This compound was synthesized following the similar procedure for 10_{OTf} (Scheme 1) starting from 11_{CI} (0.300 g, 0.485 mmol, 1.0 equiv.). After filtration and evaporation of the filtrate, the residual solid was triturated with acetonitrile (1 mL) and diethyl ether (20 mL) to get an off-white solid. The solid was further washed with diethyl ether (20 mL) to obtain the desired product (11_{OTf}) (0.341 g, 0.403 mmol, 83%) as an off-white solid. Characterization data for 11_{OTf} : ¹H NMR (CDCl₃, 360 MHz): 10.23 (bs, 2H, Im (pre-carbene H)); 9.0 (bs, 2H, Im); 8.19 (s, 2H, py); 7.56 (t, 2H, $J_{HH} = 7.9$ Hz, Dipp-Ar); 7.37 (bs, 2H, Im); 7.33 (d, 4H, $J_{HH} = 7.9$ Hz, Dipp-Ar); 2.66 (s, 3H, py-Me); 2.38 (m, 4H, Dipp- $CHMe_2$); 1.21 (d, 12H, $J_{H-H} = 6.8$ Hz, Dipp- $CHMe_2$); 1.17 (d, 12H, $J_{H-H} = 6.8$ Hz, Dipp- $CHMe_2$); 1.17 (d, 12H, $J_{H-H} = 6.8$ Hz, Dipp- $CHMe_2$); -78.67.

Complex 9 was synthesized following a modified literature procedure (Scheme 1). [10,19] Inside the glovebox, a Schlenk flask was loaded with Ru(bipy)Cl₄ (0.100 g, 0.250 mmol, 1.0 equiv.), 11 (0.212 g, 0.250 mmol, 1.0 equiv.), ethylene glycol (3 mL) and a stir-bar. The flask was sealed with a rubber septum, taken out of the glovebox, and connected to a Schlenk line under N2. Then the reaction mixture was refluxed while stirring for 1.5 h. After cooling to room temperature, saturated aqueous NH₄Cl solution (3 mL) was added to the reaction mixture. A red-brown solid precipitated out, the solid was collected on a Büchner funnel by filtration, washed with water and dried under vacuum. Then a separate Schlenk flask was loaded with the dried brown solid, zinc granules (0.032 g, 0.489 mmol, 1.3 equiv.), ethanol (40 mL) and a stir-bar. The flask was connected to a Schlenk line under N2 and the reaction mixture was refluxed while stirring for 1 h. After cooling to room temperature, ethanol was evaporated under vacuum, the crude product was purified by column (silica gel) chromatography using 0-10% methanol in dichloromethane. It was further purified by recrystallization from vapor diffusion of diethyl ether into acetonitrile solution of the compound to get a brown solid as the desired product (9) (0.045 g, 0.045 mmol, 18%). Single crystals were grown by vapor diffusion of diethyl ether into acetonitrile solution of the compound. Characterization data for 9: ¹H NMR (DMSO- d_6 , 500 MHz): δ 8.97 (d, 1H, $J_{HH} = 5.0$ Hz, bpy); 8.64 (d, 2H, $J_{HH} = 2.0$ Hz, Im); 8.27 (d, 1H, $J_{HH} = 8.0$ Hz, bpy); 8.13 (s, 2H, py); 7.93 (d, 1H, J_{HH} = 8.0 Hz, bpy); 7.70 (t, 1H, J_{HH} = 8.0 Hz, bpy); 7.59 (d, 2H, $J_{\rm HH} = 2.0$ Hz, Im); 7.55 (d, 1H, $J_{\rm HH} = 5.0$ Hz, bpy); 7.35 (t, 1H, $J_{\rm HH}$ = 8.0 Hz, bpy); 7.09 (t, 1H, J_{HH} = 7.0 Hz, bpy); 7.03 (m, 2H, Dipp-Ar); 6.96 (d, 2H, J_{HH} = 8.0 Hz, Dipp-Ar); 6.72 (t, 1H, J_{HH} = 7.0 Hz, bpy); 6.63 (d, 2H, $J_{HH} = 8.0$ Hz, Dipp-Ar); 3.08 (m, 2H, Dipp- $CHMe_2$); 2.82 (s, 3H, py-Me); 1.17 (d, 6H, J_{HH} = 6.5 Hz, Dipp-CHMe₂); 1.11 (m, 2H, Dipp-7.0 Hz, Dipp-CH Me_2); 0.35 (d, 6H, $J_{HH} = 6.5$ Hz, Dipp-CH Me_2);. NMR (DMSO- d_6 , 339 MHz): δ –77.76. HRMS (ESI, positive) calculated for $RuC_{46}H_{51}N_7Cl$ [M - $(CF_3SO_3)^-$]⁺: 838.2938 and found 838.2950. Elemental compositions calculated for $RuC_{47}H_{51}N_7O_3F_3SCl$ (M): C =57.16%, H = 5.21%, N = 9.93%; found C = 56.88%, H = 5.26%, N = 5.26%9.85%. UV–vis: $\lambda_{max} = 481$ nm, $\epsilon = 8400$ M $^{-1}$ cm $^{-1}$. FTIR (ATR, cm $^{-1}$): 3070, 2963, 2928, 2868, 1630, 1575, 1549, 1478, 1463, 1444, 1420, 1404, 1384, 1363, 1330, 1254, 1241, 1224, 1192, 1154, 1059, 1030, 988, 951, 878, 829, 802, 787, 757, 729, 704, 662, 636, 597, 572, 560, 517, 464, 426.

2.3. Crystallography

2.3.1. Experimental determination of the single crystal structure for 8

Single dark red block-shaped crystals of **8** were grown by vapor diffusion of diethyl ether into acetonitrile solution of the compound. A suitable crystal with dimensions of $0.30 \times 0.20 \times 0.10 \text{ mm}^3$ was selected and mounted on a suitable support on an XtaLAB Synergy R, DW system, HyPix diffractometer. The crystal was kept at a steady T=100.01(10) K during data collection. The structure was solved with the ShelXT [20]

structure solution program using the Intrinsic Phasing solution method and by using Olex2 [21] as the graphical interface. The model was refined with version 2018/3 of ShelXL 2018/3 [20,22] using Least Squares minimization on F^2 . Data were measured using ω scans of 0.5 per frame for 5.0 s using Mo K_{α} radiation. The total number of runs and images was based on the strategy calculation from the program CrysAlisPro 1.171.40.67a (Rigaku OD, 2019) and the unit cell was refined using CrysAlisPro 1.171.40.67a (Rigaku Oxford Diffraction, 2019) on 54,573 reflections, 82% of the observed reflections. The maximum resolution that was achieved was $\theta = 33.423^{\circ}$ (0.65 Å). The diffraction pattern was indexed. Data reduction, scaling, and absorption corrections were performed using CrysAlisPro 1.171.40.67a (Rigaku Oxford Diffraction, 2019). The final completeness is 99.90% out to 33.423° in θ . A gaussian absorption correction was performed using CrysAlisPro 1.171.40.67a (Rigaku Oxford Diffraction, 2019). Numerical absorption correction based on gaussian integration over a multifaceted crystal model. Empirical absorption correction using spherical harmonics as implemented in SCALE3 ABSPACK. The absorption coefficient μ of this material is 0.530 mm⁻¹ at this wavelength ($\lambda = 0.711 \text{ Å}$) and the minimum and maximum transmissions are 0.669 and 1.000. The structure was solved and the space group P-1 (# 2) determined by the ShelXT structure solution program using Intrinsic Phasing and refined by Least Squares using version 2018/3 of ShelXL 2018/3. [20,22] All non-hydrogen atoms were refined anisotropically. Hydrogen atom positions were calculated geometrically and refined using the riding model. Hydrogen atom positions were calculated geometrically and refined using the riding model.

Crystal Data for 8: $C_{42}H_{40}ClF_3N_8O_3RuS$, $M_r = 930.40$, triclinic, P-1 (No. 2), a = 9.57190(10) Å, b = 15.14400(10) Å, c = 15.88160(10) Å, $\alpha = 78.7740(10)^\circ$, $\beta = 82.8980(10)^\circ$, $\gamma = 75.1410(10)^\circ$, V = 2175.98(3) Å³, T = 100.01(10) K, Z = 2, Z' = 1, μ (Mo K_{α}) = 0.530, 66,805 reflections measured, 15,118 unique ($R_{int} = 0.0249$) which were used in all calculations. The final wR_2 was 0.0836 (all data) and R_1 was 0.0299 (I > 2 σ (I)).

2.3.2. Experimental determination of the single crystal structure for 9

Single clear dark red plate crystals of 9 were grown by vapor diffusion of diethyl ether into acetonitrile solution of the compound. A suitable crystal with dimensions $0.24 \times 0.11 \times 0.11 \text{ mm}^3$ was selected and mounted on a XtaLAB Synergy R, DW system, HyPix diffractometer. The crystal was kept at a steady T = 100.00(10) K during data collection. The structure was solved with the ShelXT [20] solution program using dual methods and by using Olex2 1.3-alpha [21] as the graphical interface. The model was refined with ShelXL 2018/3 [20] using full matrix least squares minimization on F². Data were measured using ω scans using Mo K_{α} radiation. The diffraction pattern was indexed and the total number of runs and images was based on the strategy calculation from the program CrysAlisPro (Rigaku, V1.171.40.80a, 2020). The maximum resolution that was achieved was $\theta = 33.430^{\circ}$ (0.65 Å). The unit cell was refined using CrysAlisPro (Rigaku, V1.171.40.80a, 2020) on 94,130 reflections, 65% of the observed reflections. Data reduction, scaling, and absorption corrections were performed using CrysAlisPro (Rigaku, V1.171.40.80a, 2020). The final completeness is 100.00% out to 33.430° in θ . A gaussian absorption correction was performed using CrysAlisPro 1.171.40.80a (Rigaku Oxford Diffraction, 2020). Numerical absorption correction based on gaussian integration over a multifaceted crystal model Empirical absorption correction using spherical harmonics, implemented in SCALE3 ABSPACK scaling algorithm. The absorption coefficient μ of this material is 0.507 mm⁻¹ at this wavelength $(\lambda = 0.71073 \text{ Å})$ and the minimum and maximum transmissions are 0.729 and 1.000. The structure was solved and the space group P-1 (# 2) determined by the ShelXT [20] structure solution program using dual methods and refined by full matrix least squares minimization on F² using version 2018/3 of ShelXL 2018/3. [20] All non-hydrogen atoms were refined anisotropically. Hydrogen atom positions were calculated geometrically and refined using the riding model. Hydrogen atom

positions were calculated geometrically and refined using the riding model

Crystal Data for 9: $C_{47}H_{51}ClF_3N_7O_3RuS$, $M_r=987.53$, triclinic, P-1 (No. 2), a=13.05610(10) Å, b=18.8751(2) Å, c=18.8805(2) Å, $\alpha=85.5590(10)^\circ$, $\beta=81.8450(10)^\circ$, $\gamma=87.3720(10)^\circ$, V=4589.07(8) Å³, T=100.00(10) K, Z=4, Z'=2, μ (Mo $K_\alpha)=0.507$, 144,079 reflections measured, 31,500 unique ($R_{int}=0.0189$) which were used in all calculations. The final wR^2 was 0.0787 (all data) and R_1 was 0.0290 ($I \geq 2\sigma$ (1)).

2.4. $Log(D_{o/w})$ measurements

2.4.1. Materials and instruments

1-octanol and sodium phosphate (monobasic and dibasic) salts were purchased from commercial vendors and used without further purification. UV–vis absorptions were recorded using a PerkinElmer Lambda 35 UV–Vis or a JASCO Spectrometer using a cuvette of 1 cm path length. All the experiments were done under ambient conditions.

2.4.2. General procedure

1-octanol and 0.1 M phosphate buffer (pH 7.4) were mixed in a 1:1 ratio and stirred for 24 h before use to ensure that the solutions were saturated. Separation of the aqueous and organic layers gave presaturated buffer and pre-saturated octanol solutions. These presaturated buffer and octanol solutions were used for experiments to calculate both the molar absorptivity and $\log(D_{0/w})$ values of the ruthenium compounds studied herein. The procedure used to measure $\log(D_{0/w})$ was a modified "shake flask" method that was deemed acceptable for use by measuring the $\log(D_{0/w})$ at pH 7.4 of 5-fluorouracil and comparing those results to reported literature values. [23]

2.4.3. Determining the molar absorptivity values

Solutions of five different concentrations (between 10 and 100 $\mu M)$ of the ruthenium compounds were prepared and their UV–Vis absorptions were recorded. For each compound, the molar absorptivity values both in octanol and in buffer (if the compound was soluble in both the solutions) were calculated from the Beer's Law plots.

2.4.4. Determining the $log(D_{o/w})$

If a compound was insoluble in buffer and soluble in octanol, its $\log(D_{0/w})$ was assumed to be >3. As a general procedure, the ruthenium compound of interest was first dissolved in octanol with a final solution concentration between 50 and 150 μ M (depending on the solubility of the compound). A portion of this solution (5 mL) was then mixed with an equal volume of buffer and gently stirred for 24 h. Then the layers were separated, centrifuged (generally, there was no solid precipitate), and UV–vis absorptions of the solutions were recorded to determine the concentrations of ruthenium in both the aqueous and organic phases. Then, the $\log(D_{0/w})$ values were calculated following the equation given below. Values of $\log(D_{0/w})$ values were measured at least in duplicate. This procedure is similar to our past published work. [6]

$$\label{eq:log_operator} \text{log}\left(D_{\text{o/w}}\right) = \text{log}\left([Ru]_{(Org)} \Big/ [Ru]_{(Aq)}\right).$$

2.5. Cell culture

Breast epithelial adenocarcinoma cell lines MDA-MB-231 and MCF7, as well as non-tumorigenic breast epithelial cell line MCF10A (all purchased from ATCC, Manassas, VA) were seeded in 96-well plates at a density of 20,000 cells per well in 100 μL of cell culture media. Dulbecco's Modified Eagle Media (Gibco, Waltham, MA) supplemented with 10% v/v fetal bovine serum (Gibco) was used for MDA-MB-231 and MCF7, and Mammary Epithelium Basal Medium (Lonza, Basel, Switzerland) supplemented with Mammary Epithelial Cell Growth Medium SingleQuots Kit (Lonza) was used for MCF10A. Both media were

phenol red-free. The cells were treated with 100 µL of ruthenium compounds dissolved in 1% v/v DMSO/media. For the initial screening, the cells were treated with 5 µM of compounds 1-9. For EC₅₀ determination, the cells were treated with compounds with varying concentrations of 5-6 orders of magnitude. In both experiments, the compounds were incubated with the cells for 48 h in the dark. Cells were then gently washed with pH 7.2 phosphate-buffered saline (200 μ L \times 3; Gibco), remained in the dark for additional 2 h or irradiated for 2 h with white light (STASUN 200 W LED flood light, 100-256 V, 20,000 lm, 40,000 lx, irradiance: 40 mW cm⁻², total fluence: 288 J cm⁻²). All cells were then incubated in fresh media (200 μL per well) for additional 24 h in the dark. Cell viability was measured using Cell Counting Kit-8 at 460 nm according to manufacturer's protocol (Enzo Life Sciences, Farmingdale, NY). The EC₅₀ of the compounds was then determined using a nonlinear regression fit of the dose-response curve using the following formula using GraphPad Prism (v 9.3.1, La Jolla, CA):

$$A_{
m obs} = A_{
m min} + rac{A_{
m max} - A_{
m min}}{1 + 10^{(log ext{EC50} - log [ext{Ru}]\,)}}$$

where $A_{\rm obs}$ is the observed absorbance, $A_{\rm max}$ and $A_{\rm min}$ were the maximum and minimum absorbance detected, respectively. For compounds that did not yield different cytotoxicities under dark and light conditions, the above experiments were repeated in ambient light conditions. Statistical significance was determined using one-way ANOVA with post-hoc Tukey HSD test (GraphPad Prism).

2.6. Detecting Total ROS

For detecting total ROS, MDA-MB-231 cells were seeded into 12-well plates at 5×10^4 cells/well. Reactive oxygen species (ROS) production was measured using Total ROS Detection Kit according to the manufacturer's protocol (Enzo Life Sciences, Farmingdale, NY; n=3). Total ROS in cells were measured via flow cytometry following overnight incubation in 5 μM of each compound and 2 h of irradiation with white light where indicated. Flow cytometry was performed using an S3e Fluorescence Activated Cell Sorter (Bio-Rad, Hercules, CA) and analyzed using FlowJo (v10.7.1) ANOVA analysis was performed using GraphPad Prism 9.

3. Results and discussion

3.1. Synthesis

The synthesis of various pincer ligands and their Ru complexes (in 1, 6, 7) have been reported previously (Fig. 1). [9,10] In brief, complex 1 was made by treating $[(\eta^6\text{-cymene})\text{RuCl}_2]_2$ with the pincer ligand precursor and a base in acetonitrile, but 6 and 7 were made via a different route using $\text{Ru}(bpy)\text{Cl}_4$ and the pincer precursor in a method similar to Scheme 1. We note that an alternative method for making [(CNC)Ru (bpy)X]^{n+} complexes was recently reported by us involving treatment of [(CNC)Ru(CH_3CN)_2Cl](CF_3SO_3) with a diimine (e.g. bpy) in methanol. [24] In a similar fashion, complexes 2 and 4, [(CNC)Ru(bpy)Cl] (CF_3SO_3), were prepared as reported separately. [11,12] Complexes 2 and 4 were then treated with Ag(CF_3SO_3) in acetonitrile to remove the halide by salt metathesis and yield the dicationic complexes 3 and 5, respectively. [11,12]

It has been a long-standing goal of our group to introduce bulky aryl wingtip groups (e.g. Mes, Dipp in Fig. 1) on the NHC rings of our CNC pincer ligands. Bulky aryl groups are expected to be beneficial for both catalysis in terms of site isolation and for anticancer applications in terms of improved lipophilicity and cellular uptake. An initial goal was to synthesize [(CNC)Ru(bpy)Cl]⁺ complexes with bulky aryl wingtips and a methoxy group on the CNC ligand for comparison to 2–7 and for the design of catalysts. [10] However, efforts to synthesize CNC ligands containing bulky aryl wingtip groups and methoxy substituents were not

successful. At elevated temperatures (150 °C), treatment of 1-aryl imidazole with 2,6-difluoro-4-methoxy-pyridine (similar to Scheme 1) led to a nucleophilic attack at the methoxy carbon on the pyridyl ring producing a 1-aryl-3-methyl imidazolium salt (a demethylation product) in an undesired side reaction. Thus, CNC-pincers with bulky aryl groups have required the use of H or methyl on the pyridine ring of the CNC pincer (in 8 and 9) since methoxy substituents have been synthetically inaccessible.

In contrast, the reaction between 2,6-dihalo-4-R-pyridine (R = H, Me) and 1-aryl imidazole (aryl = Mes, Dipp) at 150 °C in a sealed tube proceeded smoothly to yield 10_{Br} or 11_{Cl} (Scheme 1) in 20–30% yield. These bis(imidazolium)-pyridine derivatives were then converted from the halide salt to the triflate salt (10_{OTf} or 11_{OTf} in 93 or 83% yield, respectively) by metathesis with Ag(CF₃SO₃). Treatment of 10_{OTf} or 11_{OTf} with Ru(bpy)Cl₄ in ethylene glycol yielded a Ru(IV) complex that was then reduced with Zn in ethanol to produce 8 and 9 in 34 and 18% yield, respectively (Scheme 1). [10,19] These complexes were characterized by 1 H and 19 F NMR, HRMS, IR, elemental analysis methods and by crystallography as described below.

3.2. Single crystal X-ray diffraction

The crystal structures of both 8 and 9 are shown in Fig. 2. Both structures feature octahedral Ru(II) centers with bond angles around the metal reflecting the chelate ring constraints. The smallest angles in 8 are 77-78° involving C(NHC)-Ru-N3(py) within the CNC pincer. Similar angles are present in 9. The bond angles and bond distances (Table 1) are unremarkable and consistent with those seen in other similar complexes including 2-7. [10,11] Ru-C(NHC) distances in 8 and 9 are typically around ~ 2.05 Å though they range from 2.044(1) Å to 2.073(1) Å. Ru—N distances are typically \sim 2.00 Å for the py (CNC pincer) and \sim 2.03 Å (N7) and \sim 2.07 Å (N6). Ru—Cl distances are \sim 2.44 Å which is similar to the analogous angle in 2, 4, and 6. Although sterically bulky Mes and Dipp ligands are used in 8 and 9, respectively, the bond angles and bond lengths appear unperturbed by steric interactions. Examination of the space-filling models from the crystal structure reveals that while the aryl wingtips are proximate to the bpy ring, these interactions are not close enough to alter the Ru-C or Ru-N distances in 8 and 9 vs. 2-7.

Table 1 Selected bond distances (\mathring{A}) involving the ruthenium center in 8 and 9.

	Ru-C1	Ru-C11	Ru-N3	Ru-Cl	Ru-N6	Ru-N7
8	2.048(1)	2.053(1)	2.005(1)	2.4480(3)	2.067(1)	2.034(1)
9 ^a	2.054(1)	2.044(1)	2.004(1)	2.4407(5)	2.057(1)	2.038(1)
	2.073(1)	2.061(1)	2.006(1)	2.4392(6)	2.061(1)	2.039(1)

^a There are two inequivalent molecules in the asymmetric unit of 9.

3.3. Cellular toxicity studies vs. Cancer cells

Initially, compounds 1–9 were screened for toxicity under both dark and light conditions using MCF7 breast cancer cells. These compounds were originally designed as catalysts for CO_2 reduction, [9–11,24,25] but here they were repurposed as potential cancer cell chemotherapeutics. Complexes 1–3 and 5 at 5 μ M showed negligible cellular toxicity from our screening data. The screening of complex 4 showed some modest anticancer activity (Fig. S17), but this was not further studied due to the greater potency of 6–9 as our four lead compounds. It appears that increased lipophilic character imparted by aryl wingtips on the NHC ligands has improved the cytotoxicity (Fig. 1).

Two of these compounds (6 and 9) showed cytotoxicity in the dark, but they were not light-activated. These compounds were subsequently evaluated under ambient lighting conditions (Table 2 and Fig. 3) since the screening data showed the same toxicity under both light and dark conditions. These compounds displayed EC50 values from 1 to 5 μM vs.

Table 2 EC_{50} data for treatment with 6 and 9 under ambient light conditions. Compounds 6 and 9 were shown to have the same toxicity under light and dark conditions from the screening data.

Ru cmpd	MCF7 SI ^a (Breast (MCF7) Cancer)		MDA-MB-231 (Breast CSC)		
			EG (10		EC () ()
	EC ₅₀ (μM)		EC ₅₀ (μM)		EC ₅₀ (μM)

^a Selectivity Index (SI) = EC_{50} normal / EC_{50} cancer.

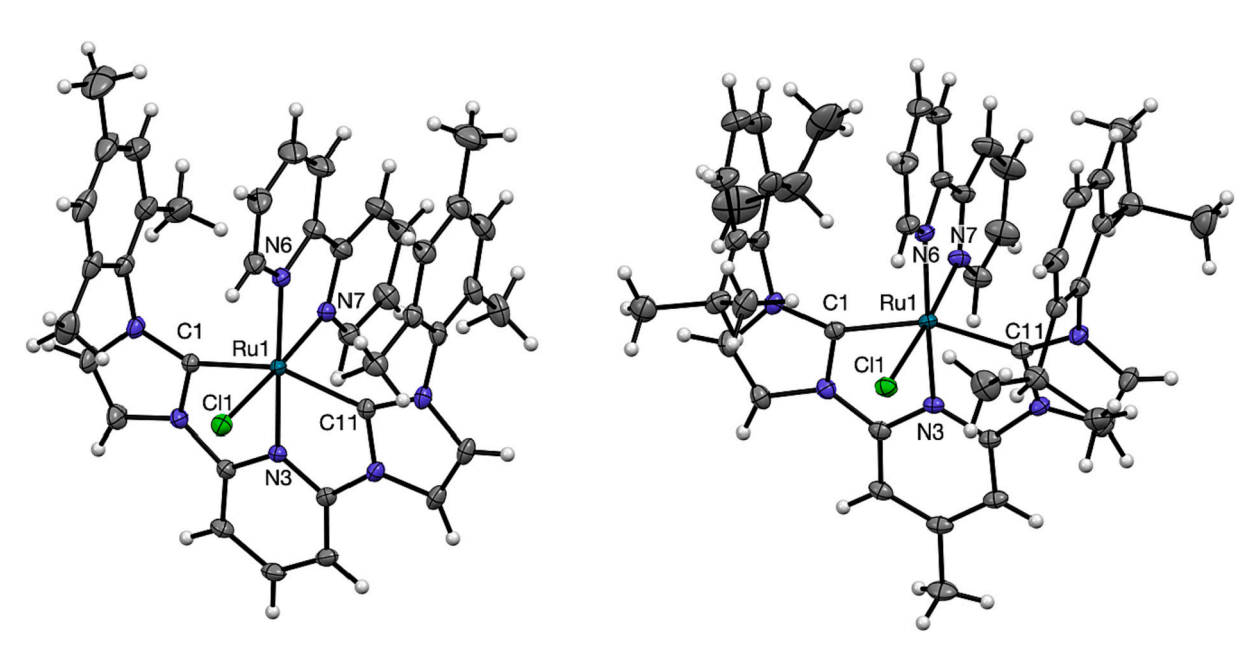


Fig. 2. Molecular diagrams of 8 (left) and 9 (right) from the crystallographic data. Triflate counter anions and solvent molecule if applicable (CH_3CN for 8) are hidden for clarity. Thermal ellipsoids are drawn at 50% probability level. Colour code: grey = carbon, white = hydrogen, blue = nitrogen, green = chlorine, teal = ruthenium. While there are two inequivalent molecules in the asymmetric unit for 9, only one is shown above. (For interpretation of the references to colour in this figure legend, the reader is referred to the web version of this article.)

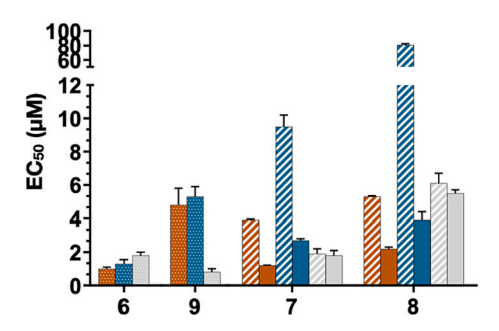


Fig. 3. Graphic summary of the EC_{50} data (**orange** = MCF7, **blue** = MDA-MB-231, **grey** = MCF10A). Compounds **6** and **9** showed the same toxicity under light and dark conditions, and so they were evaluated under ambient lighting conditions (left, dotted bars indicate ambient lighting). The photocytotoxic compounds **7** and **8** were evaluated under dark (stripes) and light (solids) conditions (right). (For interpretation of the references to colour in this figure legend, the reader is referred to the web version of this article.)

two cancer cell types (MCF7 and MDA-MB-231). MDA-MB-231 are considered breast "cancer stem-like cells" (CSC) cells, which are believed to have tumor-initiating potential and are therefore implicated in tumor relapse and metathesis. [26–31] Targeting CSCs is therefore a key goal for many researchers. Thus, the similar efficacy of $\bf 6$ and $\bf 9$ vs. MCF7 and MDA-MB-231 is encouraging. However, these compounds were unfortunately also toxic towards normal cells (MCF10A) with selectivity indices of 1.4–1.8 for $\bf 6$ and $\bf \sim 0.15$ for $\bf 9$ (Table 2). As such, $\bf 6$ and $\bf 9$ are not especially promising for future studies.

Complexes 7 and 8 were light-activated with improved cytotoxicity upon white light irradiation from our screening data. Thus, light and dark EC $_{50}$ values were measured for these compounds (Table 3 and Fig. 3). Light EC $_{50}$ values ranged from 1 to 4 μ M vs. the two cancerous cell lines. The phototoxicity index (EC $_{50}$ dark/EC $_{50}$ light, or PI value) is typically considered the best metric for evaluating a light activation chemotherapeutic agent. This metric would suggest that 8 is most promising with a PI value of ~21 vs. MDA-MB-231. Furthermore, complex 8 exhibited significant changes in PI value from cell line to cell line for reasons that are currently unclear, but shows promise to be further developed as a potential CSC-specific compound.

Given the promising activity of compounds 6–9 vs. cancer cells, we investigated the biological mode of action by measuring ROS in MDA-MB-231 cells (Fig. 4). Complexes 6 and 9 were cytotoxic in the dark and were not light activated, as such they were evaluated for ROS in ambient lighting. Complex 6 did not produce significant quantities of ROS but complex 9 showed ~40% ROS positive cells (p < 0.01 relative to control). ROS production in the dark is by an unknown mechanism, but the literature would suggest it could be driven by Fenton-like chemistry or other redox processes catalyzed by 9. [32,33] The differences between 6 and 9 may relate to increased lipophilicity of 9 (see below for further discussion and $\log(D_{0/w})$ values) which leads to better uptake for 9 and may influence where it localizes in the cell. Lipophilic molecules often localize in the mitochondria of cells. [2]

Complexes 7 and 8 were light activated and were tested in the dark and upon irradiation with visible light. ROS levels upon treatment with 7 were low (similar to the control) and not statistically significant. Light activation of 7 may involve $\mathrm{CH_3CN}$ ligand loss and binding to biological

targets as suggested by Fig. S16 and by a lack of ROS production. Upon cell treatment with $\bf 8$ and light irradiation $\sim\!6\%$ of the cells were ROS positive cells (p < 0.001 with respect to both $\bf 8$ in the dark and the control with no Ru complex). This would suggest that light is leading to ROS production with $\bf 8$ which could be by singlet oxygen production or other mechanisms. [2,3] Further studies on the biological targets of these compounds and their mode of action (including which ROS species are formed) could be performed in the future.

We note that while complexes 8 and 9 produce ROS the percentage of ROS positive cells is much lower here than in our past work which featured a Ru complex which led to $\sim\!\!90\%$ ROS positive cells for the same assay and correspondingly a higher photocytotoxicity index (EC50_light = 4 μ M, PI = 120 vs. MCF7) than observed herein. [3,5] Again, what separates complexes 8 and 9 from the others (1–7) is their lipophilicity (see below), which may drive localization in the mitochondria and ROS production.

3.4. $Log(D_{o/w})$ measurements as an estimate of cellular uptake

 $Log(D_{o/w})$ measurements (Table 4) have been performed by UV–Vis spectroscopy to estimate molecular lipophilicity to determine a propensity for cellular uptake by passive diffusion. Complexes 1–5 are very hydrophilic with negative $log(D_{o/w})$ values which suggests poor uptake through the lipophilic cellular lipid bilayer. This alone may explain the lack of toxicity for 1–5.

In contrast, complexes 6–9 are more lipophilic with positive $\log(D_{0/w})$ values (Table 4) and a preference for octanol over water. A few trends have been revealed from this work. The use of Cl vs. CH₃CN as the monodentate ligand in 6 vs. 7 served to decrease the $\log(D_{0/w})$ value from 0.7 to 0.5, due to the increased positive charge for 7 (2+) vs. 6 (1+). Complex 9 is very lipophilic with the estimate of $\log(D_{0/w}) > 3$ (no solubility in water observed alongside excellent solubility in octanol). However, complex 8 appears to be our most promising compound ($\log(D_{0/w}) = 1.3$) due to favorable enough uptake combined with light activation. We note that ROS production was only observed for 8 and 9 (see above) and that perhaps increased lipophilicity for these complexes could be driving localization in the mitochondria which could lead to increased oxidative stress and the observed toxicity.

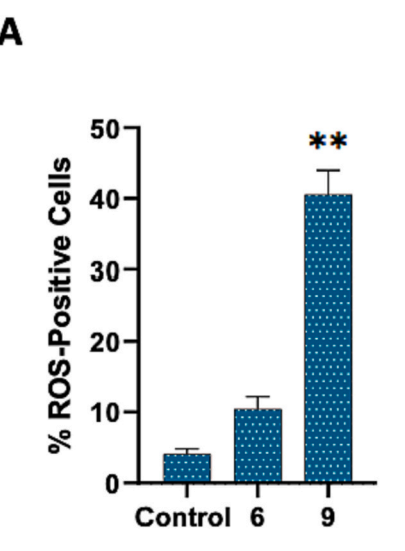
4. Conclusion

Nine compounds are reported herein, of which four displayed activity vs. cancer cells at micromolar concentrations. Several trends are apparent from this data. Modification of the ligand scaffold from an imidazole based NHC ring to a benzimidazole bases NHC ring on the CNC pincer led to some modest activity for compound 4 from the screening data. Of compounds 1-5, compounds 4 and 5 were the most lipophilic due to the benzimidazole based NHC ring. This lipophilicity was increased further in 6 and 7 by inclusion of phenyl wingtip groups on the NHC ring. Compound 7 was light activated by a mechanism that appears to involve light triggered ligand loss potentially followed by binding to biological targets. Compound 8 was also light activated with ROS production increasing upon irradiation with PI = 21 and EC_{50 light} = 4 μM vs. MDA-MB-231. Complex 8 can be compared to compounds similar in structure including a [Ru(CNC)2] complex (featuring an anionic CNC ligand due to a carboxylate group) with PI as high as 86 (405 nm light) and a [Ru(CNN)₂]²⁺ complex with PI as high as 37

Table 3 EC_{50} data for treatment with 7 and 8 in the dark and upon irradiation for two hours with white light.

Ru cmpd	MCF7 (Breast Cancer)			MDA- MB-231 (Breast CSC)			MCF10A (Normal)		
	EC _{50 Dark} (μM)	EC _{50 Light} (μM)	PI ^a	EC _{50 Dark} (μM)	EC _{50 Light} (μM)	PI ^a	EC _{50 Dark} (μM)	EC _{50 Light} (μM)	PI ^a
7	3.9(6)	1.2(1)	3.3	9.5(7)	2.7(1)	3.5	1.9(3)	1.8(3)	1.1
8	5.3(1)	2.2(1)	2.4	81(1)	3.9(5)	21	6.1(6)	5.5(2)	1.1

^a The phototoxicity index (PI) is the ratio of EC_{50} in the dark to EC_{50} in the light.



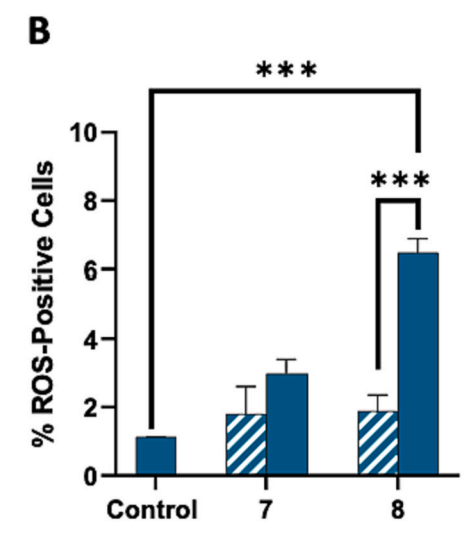


Fig. 4. ROS indicators in MDA-MB-231. Panel **A** shows ROS detected in ambient light conditions in the absence of Ru compound (control) and with 5 mM of **6** and **9**. Panel **B** shows ROS detected in cells incubated in the dark, represented by striped bars, and solid bars represent cells incubated in the dark and subsequently irradiated with visible white light. The one-way ANOVA test was performed to determine statistical significance where ** = p < 0.01 and *** = p < 0.001.

Table 4 Log($D_{o/w}$) values at pH 7.4 for selected compounds.

Ru cmpd	Log(D _{o/w}) at pH 7.4		
1	< -3 ^a		
2	$< -3^{a} < -3^{a}$		
3	$< -3^{a}$		
4	-0.8(1)		
5	-0.05(9)		
6	0.7(2)		
7	0.5(1)		
8	1.3(1)		
9	$>3^{\mathrm{b}}$		

 $^{^{\}rm a}$ Log(D_{o/w}) <-3 indicates good solubility in aqueous buffer and no detectable (by UV–Vis) solubility in octanol.

(indigo light) vs. HL60 leukemia cells. [8] Both of these complexes were shown to generate singlet oxygen and induce DNA damage. Of course, given the difference in cell lines, there is limited meaning to this comparison except that PI values are the same order of magnitude as for 8. Compound 9 was cytotoxic but not light activated with ROS production (in up to 40% of cells) observed. Overall, complex 8 was most promising due to light activation combined with the inclusion of lipophilic aryl wingtip groups on the NHC ring which leads to an improved $log(D_{\alpha/w})$ values that would favor cellular uptake by passive diffusion. Our study also suggests that the CNC's pyridine substituent can be varied from an electron donating OMe group (in 6 and 7) to the electronically closer to neutral H (8) or Me (9) groups which leads to an improvement in photocytotoxicity (for 8) or cytotoxicity (for 9). In fact, while ROS levels were generally low relative to our past work, [3] they were greatest for complexes 8 and 9. Thus, future studies will focus on lipophilic Ru complexes electronically similar to 8 and 9 as well as studies on their mode of action. [8,34]

Author contributions

Sun, Yifei: data curation; formal analysis; writing - original draft.Das, Sanjit: data curation; formal analysis; writing - original draft, review and editing.

Brown, Spenser R.: data curation; formal analysis; supervision;

writing - original draft, review and editing.

Blevins, Emily R.: data curation; formal analysis; writing - original draft.

Qu, Fengrui: data curation; formal analysis; writing - original draft. **Ward, Nicholas A.**: data curation; formal analysis; writing - original raft

Gregory, Shawn Aiden: data curation; formal analysis.

Boudreaux, Chance M.: data curation; formal analysis.

Kim, Yonghyun: writing - review and editing; supervision; funding acquisition.

Papish, Elizabeth T.: conceptualization; writing - original draft, review and editing; supervision; funding acquisition.

All authors have reviewed the final manuscript and approve of its submission.

Declaration of Competing Interest

The authors declare that they have no known competing financial interests or personal relationships that could have appeared to influence the work reported in this paper.

Data availability

Data will be made available on request.

Acknowledgements

We gratefully acknowledge support from the NIH (R15-GM132803-01 and R15-GM132803-02) to ETP and YK. SRB was supported by the US Department of Education as a GAANN Teaching Fellow (P200A180056). We thank NSF MRI program (CHE 1726812, PI Cassady) and UA for the purchase of a MALDI TOF/TOF MS and Dr. Qiaoli Liang for MS experimental work. We thank Dr. Ken Belmore for assistance with the NMR experiments. We thank NSF CHE MRI 1828078 and UA for the purchase of the SC XRD instrument. We thank NSF CHE MRI 1919906 and UA for the purchase of an NMR spectrometer. SAG and ERB participated in this project via the NSF REU program (EEC-1950855, PI Summers). We thank Dr. Igor Fedin for the use of a UV–Vis instrument.

Appendix A. Supplementary data

CCDC 2179613-2,179,614 contain the supplementary

 $^{^{\}rm b}$ Log(D_{0/w}) > 3 indicates good solubility in octanol and no detectable (by UV–Vis) solubility in aqueous buffer

crystallographic data for this paper. These data can be obtained free of charge via www.ccdc.cam.ac.uk/data_request/cif, or by emailing data_request@ccdc.cam.ac.uk, or by contacting The Cambridge Crystallographic Data Centre, 12 Union Road, Cambridge CB2 1EZ, UK; fax: +441,223 336,033. Supplementary data to this article can be found online at [https://doi.org/10.1016/j.jinorgbio.2022.112110].

References

- [1] K.T. Hufziger, F.S. Thowfeik, D.J. Charboneau, I. Nieto, W.G. Dougherty, W. S. Kassel, T.J. Dudley, E.J. Merino, E.T. Papish, J.J. Paul, J. Inorg. Biochem. 130 (2014) 103–111
- [2] O. Oladipupo, S.R. Brown, R.W. Lamb, J.L. Gray, C.G. Cameron, A. R. DeRegnaucourt, N.A. Ward, J.F. Hall, Y. Xu, C.M. Petersen, F. Qu, A.B. Shrestha, M.K. Thompson, M. Bonizzoni, C.E. Webster, S.A. McFarland, Y. Kim, E.T. Papish, Photochem. Photobiol. 98 (2022) 102–116.
- [3] F. Qu, R.W. Lamb, C.G. Cameron, S. Park, O. Oladipupo, J.L. Gray, Y. Xu, H. D. Cole, M. Bonizzoni, Y. Kim, S.A. McFarland, C.E. Webster, E.T. Papish, Inorg. Chem. 60 (2021) 2138–2148.
- [4] F. Qu, K. Martinez, A.M. Arcidiacono, S. Park, M. Zeller, R.H. Schmehl, J.J. Paul, Y. Kim, E.T. Papish, Dalton Trans. 47 (2018) 15685–15693.
- [5] F. Qu, S. Park, K. Martinez, J.L. Gray, F.S. Thowfeik, J.A. Lundeen, A.E. Kuhn, D. J. Charboneau, D.L. Gerlach, M.M. Lockart, J.A. Law, K.L. Jernigan, N. Chambers, M. Zeller, N.A. Piro, W.S. Kassel, R.H. Schmehl, J.J. Paul, E.J. Merino, Y. Kim, E. T. Papish, Inorg. Chem. 56 (2017) 7519–7532.
- [6] S. Park, J.L. Gray, S.D. Altman, A.R. Hairston, B.T. Beswick, Y. Kim, E.T. Papish, J. Inorg. Biochem. 203 (2020), 110922.
- [7] E.T. Papish, O. Oladipupo, Curr. Opin. Chem. Biol. 68 (2022), 102143.
- [8] R.T. Ryan, K.C. Stevens, R. Calabro, S. Parkin, J. Mahmoud, D.Y. Kim, D. K. Heidary, E.C. Glazer, J.P. Selegue, Inorg. Chem. 59 (2020) 8882–8892.
- [9] W. Yao, S. Das, N.A. DeLucia, F. Qu, C.M. Boudreaux, A.K. Vannucci, E.T. Papish, Organometallics 39 (2020) 662–669.
- [10] S. Das, R.R. Rodrigues, R.W. Lamb, F. Qu, E. Reinheimer, C.M. Boudreaux, C. E. Webster, J.H. Delcamp, E.T. Papish, Inorg. Chem. 58 (2019) 8012–8020.
- [11] L.A. Hunt, S. Das, D. Nugegoda, R.W. Lamb, M.T. Figgins, F. Qu, C.E. Webster, N. I. Hammer, E.T. Papish, J.H. Delcamp, ACS Catal. (2022) (submitted 11/6/22).
- [12] S. Das, PhD Thesis: The Development of Photocatalysts for Carbon Dioxide Reduction: From Sensitized to Self-Sensitized Catalysis and Catalyst Immobilization, The University of Alabama, Tuscaloosa, AL, 2021.

- [13] L. Zeng, Y. Chen, H. Huang, J. Wang, D. Zhao, L. Ji, H. Chao, Chem. Eur. J. 21 (2015) 15308–15319.
- [14] S. Tardito, I. Bassanetti, C. Bignardi, L. Elviri, M. Tegoni, C. Mucchino, O. Bussolati, R. Franchi-Gazzola, L. Marchiò, J. Am. Chem. Soc. 133 (2011) 6235–6242.
- [15] M.J. Chow, M.V. Babak, D.Y.Q. Wong, G. Pastorin, C. Gaiddon, W.H. Ang, Mol. Pharm. 13 (2016) 2543–2554.
- [16] L. Tabrizi, H. Chiniforoshan, Dalton Trans. 45 (2016) 18333-18345.
- [17] A.A. Danopoulos, A.A.D. Tulloch, S. Winston, G. Eastham, M.B. Hursthouse, Dalton Trans. (2003) 1009–1015.
- [18] R.A. Krause, Inorg. Chim. Acta 22 (1977) 209-213.
- [19] L.-H. Chung, K.-S. Cho, J. England, S.-C. Chan, K. Wieghardt, C.-Y. Wong, Inorg. Chem. 52 (2013) 9885–9896.
- [20] G.M. Sheldrick, Acta Cryst A71 (2015) 3-8.
- [21] O.V. Dolomanov, L.J. Bourhis, R.J. Gildea, J.A.K. Howard, H. Puschmann, J. Appl. Crystallogr. 42 (2009) 339–341.
- [22] G.M. Sheldrick, Acta Cryst A64 (2008) 112-122.
- [23] G.M.M. El Maghraby, A.C. Williams, B.W. Barry, Int. J. Pharm. 292 (2005) 179–185.
- [24] S. Das, D. Nugegoda, W. Yao, F. Qu, M.T. Figgins, R.W. Lamb, C.E. Webster, J. H. Delcamp, E.T. Papish, Eur. J. Inorg. Chem. 2022 (2022), e202101016.
- [25] S. Das, D. Nugegoda, F. Qu, C.M. Boudreaux, P.E. Burrow, M.T. Figgins, R. W. Lamb, C.E. Webster, J.H. Delcamp, E.T. Papish, Eur. J. Inorg. Chem. 2020 (2020) 2709–2717.
- [26] M. Antonelli, F. Strappazzon, I. Arisi, R. Brandi, M. D'Onofrio, M. Sambucci, G. Manic, I. Vitale, D. Barila, V. Stagni, Oncotarget 8 (2017) 21692–21709.
- [27] J.W. Magrath, Y. Kim, Int. J. Oncol. 51 (2017) 753-759.
- [28] T. Reya, S.J. Morrison, M.F. Clarke, I.L. Weissman, Nature 414 (2001) 105–111.
- [29] L. Ricci-Vitiani, D.G. Lombardi, E. Pilozzi, M. Biffoni, M. Todaro, C. Peschle, R. De Maria, Nature 445 (2007) 111–115.
- [30] N.A. Lobo, Y. Shimono, D. Qian, M.F. Clarke, Annu. Rev. Cell Dev. Biol. 23 (2007) 675–699.
- [31] Y. Kim, K.M. Joo, J. Jin, D.H. Nam, Int. J. Stem Cells 2 (2009) 109-114.
- [32] I. Kacsir, A. Sipos, A. Bényei, E. Janka, P. Buglyó, L. Somsák, P. Bai, É. Bokor, Int. J. Mol. Sci. 23 (2022).
- [33] I. Kacsir, A. Sipos, G. Ujlaki, P. Buglyó, L. Somsák, P. Bai, É. Bokor, Int. J. Mol. Sci. 22 (2021) 10454.
- [34] A. Frei, R. Rubbiani, S. Tubafard, O. Blacque, P. Anstaett, A. Felgenträger, T. Maisch, L. Spiccia, G. Gasser, J. Med. Chem. 57 (2014) 7280–7292.